INTERNATIONAL JOURNAL FOR NUMERICAL METHODS IN ENGINEERING
Int. J. Numer. Meth. Engng 2009; **77**:1–29
Published online 29 July 2008 in Wiley InterScience (www.interscience.wiley.com). DOI: 10.1002/nme.2387

Fast integration and weight function blending in the extended finite element method

Giulio Ventura[1,*,†,‡], Robert Gracie[2] and Ted Belytschko[2]

[1]*Department of Structural Engineering and Geotechnics, Politecnico di Torino, 10129 Torino, Italy*
[2]*Department of Mechanical Engineering, Northwestern University, Evanston, IL 60208, U.S.A.*

SUMMARY

Two issues in the extended finite element method (XFEM) are addressed: efficient numerical integration of the weak form when the enrichment function is self-equilibrating and blending of the enrichment. The integration is based on transforming the domain integrals in the weak form into equivalent contour integrals. It is shown that the contour form is computationally more efficient than the domain form, especially when the enrichment function is singular and/or discontinuous. A method for alleviating the errors in the blending elements is also studied. In this method, the enrichment function is pre-multiplied by a smooth weight function with compact support to allow for a completely smooth transition between enriched and unenriched subdomains. A method for blending step function enrichment with singular enrichments is described. It is also shown that if the enrichment is not shifted properly, the weighted enrichment is equivalent to the standard enrichment. An edge dislocation and a crack problem are used to benchmark the technique; the influence of the variables that parameterize the weight function is analyzed. The resulting method shows both improved accuracy and optimum convergence rates and is easily implemented into existing XFEM codes. Copyright © 2008 John Wiley & Sons, Ltd.

Received 11 March 2008; Revised 11 April 2008; Accepted 16 April 2008

KEY WORDS: enriched finite elements; partition of unity; blending; numerical integration

1. INTRODUCTION

The extended finite element method (XFEM) and the generalized FEM (GFEM) have been developed to facilitate the modeling of features and arbitrary discontinuities. In contrast to the standard

*Correspondence to: Giulio Ventura, Politecnico di Torino, Department of Structural Engineering and Geotechnics, Corso Duca degli Abruzzi 24, 10129 Torino, Italy.
†E-mail: giulio.ventura@polito.it
‡Visiting Scholar, Department of Mechanical Engineering, Northwestern University, IL, U.S.A.

Contract/grant sponsor: Office of Naval Research; contract/grant number: N00014-06-1-0505
Contract/grant sponsor: Natural Sciences and Engineering Research Council of Canada

FEM, these methods do not need fine nor special mesh structures close to the discontinuous surfaces and other features, thanks to enrichment functions capable of representing these features [1–4].

The first applications of XFEM were in the area of elastic fracture mechanics [1, 2] and many improvements and applications have been reported [5–10]. Arbitrary discontinuities were successfully modeled in [5, 11]; applications to solidification problems and two-phase fluids were given in [12]. More recent applications of the XFEM include cracks in orthotropic solids [13], multiple-scale shear bands [14], dynamic cracks in elastic–plastic media [15] and dislocation problems [16, 17]. In addition, some methods for an effective implementation of XFEM have been published in [18, 19].

An advantage of the XFEM scheme is that enrichments are local. This is not a feature unique to XFEM, but exists in other enrichment methods such as the embedded discontinuity model [20], the s-version FEM [21, 22] and the spectral overlay method [23]. Recent works coupling the s-version FEM with partition of unity [24] based methods combine many of the advantages of the XFEM/GFEM and s-version schemes [25–27].

In this work we will focus on two issues that arise in the XFEM. The first issue emanates from blending, i.e. the transition from enriched to unenriched subdomains, and the second issue concerns the effective integration of the discrete equations. Both of these issues can greatly impact the computational efficiency, accuracy and convergence rate of the XFEM.

For computational efficiency, the enrichment is usually localized to subdomains close to the discontinuity, as the introduction of enrichment functions requires additional degrees of freedom. These degrees of freedom can be defined at the nodes, at the element level or even for an entire enrichment subdomain. A blending element is any element where some but not all of the nodes of the element are enriched. The union of these elements is the blending region; the blending region separates subdomains of enriched and unenriched elements.

For many enrichment functions, the approximation space of the blending elements contains parasitic terms that introduce spurious oscillations into the solution [5, 28]. The oscillations often degrade both the accuracy and the convergence properties of the XFEM. This is especially true when dealing with lower-order elements [29]. Similarly, higher-order elements are not adversely affected by blending, as shown in [30]. We note that the global enrichment methods, such as the partition of unity method (PUM) [24], do not have blending elements. However, the computational cost of enriching all nodes is significant; hence, a local enrichment scheme is still preferred.

Blending was first discussed in [5] in terms of the ramp enrichment function. A general framework to resolve the blending problem was developed in [28]. In that work, an assumed strain formulation was adopted in the blending elements, which eliminated the parasitic terms in the approximation space. Results by this approach show both improved accuracy and optimum convergence. One significant limitation of this approach is that a linearly independent basis spanning the parasitic terms is required. For complicated enrichment functions, the determination of the basis is not trivial. For example, in [31] a space of 16 functions was used to alleviate the blending problems that arise from the use of the elastic crack enrichments introduced in [2]. In [28], a blending strategy based on increasing the order of interpolation of the blending elements by adding additional nodes was proposed for the material interface (ramp) enrichment. This method was recently extended in [32] to the elastic crack enrichments in [2]; the resulting method is more accurate than the standard XFEM and converges optimally.

An alternative method was reported in [31], where a discontinuous Galerkin approach is adopted for the blending. In this method, the domain is decomposed into fully enriched and unenriched patches, which are independently discretized. Continuity between the patches is enforced in a weak

DOI: 10.1002/nme

sense by an internal penalty method. Results show improved accuracy over the standard XFEM and optimal rates of convergence. The intrinsic XFEM [33] and the discontinuous enrichment method [34] are two other alternative enrichment methods that do not have blending.

Fries [35] has proposed a method based on a weighting of the enrichment that vanishes at the edge of the enriched subdomain. The method is strikingly simple and yields optimum convergence rates for elastic crack problems. In the first part of this paper, the method of Fries [35] is generalized for multiple interacting enrichments and the issue of shifting is examined. The underlying idea starts from the observation that, in general, the importance of the enrichment function decays with the distance from the feature. Generally, the standard finite element approximation space is able to well approximate the solution far from these features. Nevertheless, a certain number of enriched elements surrounding the discontinuity is desirable (sometimes mandatory) to improve the solution [16, 36]. The strategy is as follows: (a) begin with a standard partition of unity approximation [24], (b) multiply the original enrichment function by a monotonically decreasing weight function with compact support and (c) constrain all enriched degrees of freedom to be equal. A method for blending step function enrichments with singular enrichments is also described.

The weight function is chosen in a manner to avoid interelement discontinuities and hence has little effect on the order of quadrature required to integrate the discrete equations. This approach is similar to that proposed in the interesting work of Fries [35], but the weight function has a more general form. This generalization was motivated by applications to dislocations [16, 31], where all enriched degrees of freedom are constrained to be equal. In this case, the straightforward weighting does not always yield a good blending strategy and without proper shifting degenerates to the standard XFEM. An enrichment method was also proposed by Gifford and Hilton [37] for linear elastic cracks, although they proposed to apply it only in the elements about the crack tip and the crack had to be aligned with the edges of the elements.

The second issue considered is that of faster numerical integration in XFEM. Numerical integration of the weak form in XFEM is more complicated than that in FEM. In the standard FEM, the integrands are generally polynomials and hence are easily numerically integrated by Gauss quadrature. When the standard FEM approximation space is enriched, the integrands of the weak form are generally non-polynomial; in some cases, such as crack enrichments, the integrand is singular and/or discontinuous. Several techniques have been used to address this issue. In many works, enriched elements are decomposed into sub-cells, where the edges of the cell aligned with the discontinuity [2, 6]. Higher-order Gauss quadrature is then used in each sub-cell. To improve the accuracy and computational efficiency when numerically integrating functions containing the singular crack tip enrichments, 'polar' integration schemes have been proposed in [36, 38]. In these works a judicious selection of the sub-cells and a polar transformation of the integrand lead to a much more efficient integration scheme. An alternative method to the sub-cell integration of elements enriched by the step function, based on equivalent polynomials, was recently given in [39].

In the present work, we present an alternative integration scheme. The scheme is applicable to self-equilibrating enrichment functions, such as those of Liu *et al.* [40] and for dislocations [16, 17]. In this scheme, the standard domain forms of the integrals of the discrete equations are transformed into contour integrals over the element edges. The method is particularly effective when the integrand is singular, since numerical quadrature is then performed relatively far from the singularity.

The outline of this paper is as follows. In Section 2, we briefly recall the XFEM approximation and basic notation is introduced. In Section 3, the weighted XFEM approximation is defined;

DOI: 10.1002/nme

Section 4 examines a degenerate case, where the weighted XFEM is equivalent to the standard XFEM approximation. In Section 5, the weighted XFEM approximations for cracks and edge dislocations are presented and the enrichment strategies used in the numerical examples are defined. In Section 6, the issue of merging analytic and Heaviside step function enrichments is addressed. In Section 7, an efficient method for numerically integrating the element stiffness is presented for both shifted and non-shifted enrichments. Numerical examples for a dislocation and a crack problem are presented in Section 8 and our conclusions are given in Section 9.

2. LOCAL PARTITION OF UNITY ENRICHMENT

Consider a body Ω with boundary $\partial\Omega$ and let $\mathbf{u}(\mathbf{x})$ be the displacement field. The XFEM approximation of the displacement field is

$$\mathbf{u}(\mathbf{x}) = \sum_{I\in\mathcal{N}} N_I(\mathbf{x})\mathbf{u}_I + \sum_{J\in\mathcal{S}} N_J(\mathbf{x})\boldsymbol{\Psi}(\mathbf{x})a_J \tag{1}$$

where $\mathcal{N}$ is the set of all the nodes of the finite element mesh, $N_I(\mathbf{x})$ are the finite element shape functions and $\mathcal{S}$ is the set of enriched nodes ($\mathcal{S}\subseteq\mathcal{N}$), whose definition depends on the problem and on the enrichment function $\boldsymbol{\Psi}(\mathbf{x})$. In (1) and in the following only one enrichment function will be considered to simplify the notation. In PUMs [24], all the nodes are enriched and hence $\mathcal{S}\equiv\mathcal{N}$. The discrete equations for the nodal variables $\mathbf{u}_I$ and a_J are obtained by substituting (1) into a variational principle or weak form.

The nodal degrees of freedom $\mathbf{u}_I$ of the enriched nodes do not have the physical meaning of nodal displacements, as in the standard FEM. In order to make the application of essential boundary conditions simpler and improve blending, it was proposed in [11] that the standard XFEM approximation be shifted; hence, (1) is replaced by

$$\mathbf{u}(\mathbf{x}) = \sum_{I\in\mathcal{N}} N_I(\mathbf{x})\mathbf{u}_I + \sum_{J\in\mathcal{S}} N_J(\mathbf{x})(\boldsymbol{\Psi}(\mathbf{x}) - \boldsymbol{\Psi}(\mathbf{x}_J))a_J \tag{2}$$

where $\mathbf{x}_J$ is the position of node J. This does not ensure that the essential boundary conditions are met exactly along the edge of elements when the enrichment is active, but it often suffices.

Let $\mathcal{N}^e$ be the set of nodes of element e. Then element e is a blending element if $\mathcal{N}^e\cap\mathcal{S}\neq\mathcal{N}^e$ and $\mathcal{N}^e\cap\mathcal{S}\neq\emptyset$.

To illustrate the blending problem, reference is made to the bimaterial bar of Figure 1. The left edge of the bar is clamped and a displacement $\delta=1$ is prescribed at the right end. Young's moduli for $x<L/2$ and $x>L/2$ are $E_1=1$ and $E_2=2$, respectively. The total length of the bar is $L=1$.

The solution is obtained by minimizing the total potential energy with a single linear bar element, the displacement approximation (1) and the ramp enrichment function $\Psi(x)=\mathrm{abs}(x-L/2)$. The results are reported at the bottom of Figure 1, where we can see that the exact solution is obtained.

The solution deteriorates when more than one finite element is considered and is not significantly improved by further mesh refinement (Figure 2). The reason for this pathological behavior is that in the blending elements only one of the two element nodes is enriched, and hence the reproducing property of the partition of unity is lost [28]. An immediate explanation is found by observing the

DOI: 10.1002/nme

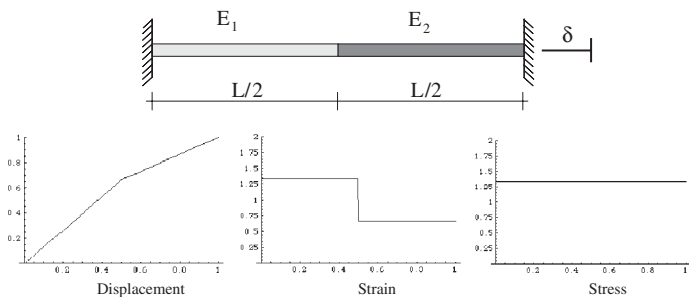

Figure 1. Bimaterial bar problem and solution with a single linear bar element enriched with the ramp enrichment function.

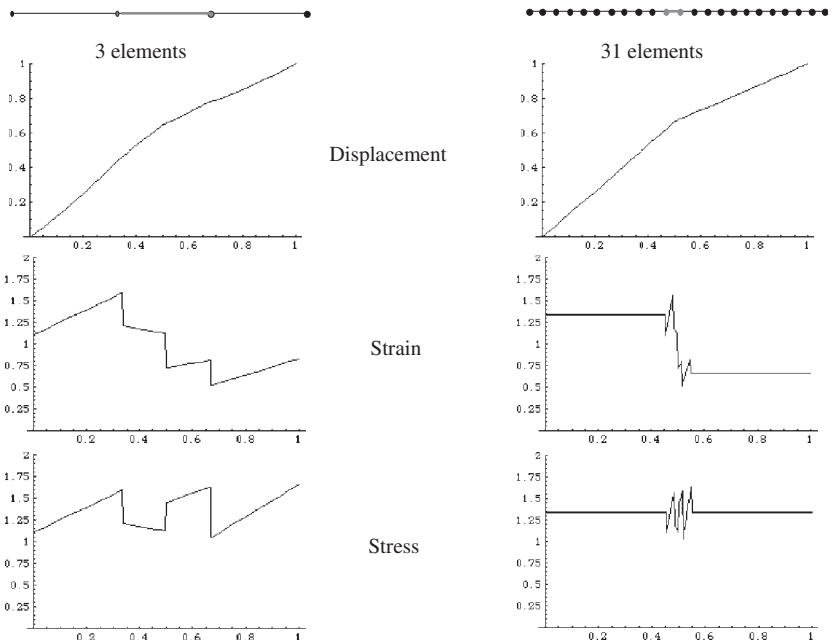

Figure 2. Blending problem for the bimaterial bar.

strain approximation in the blending element to the left of the material interface:

$$\varepsilon_x = \frac{\mathrm{d}u}{\mathrm{d}x} = \sum_{I=1}^{2} \frac{\mathrm{d}N_I}{\mathrm{d}x} u_I^e + \frac{\mathrm{d}N_2}{\mathrm{d}x} \Psi a_2^e + N_2 \frac{\mathrm{d}\Psi}{\mathrm{d}x} a_2^e \tag{3}$$

and specifically the terms associated with Ψ and $\Psi_{,x}$. These terms cause the zig-zag behavior seen in Figure 2. The first term in (3) is the standard finite element strain and is a constant. The second and third terms are the enrichment part of the strain approximation and it can be seen that the enriched part of the strain approximation cannot reproduce a constant strain field. In fact, the approximation (3) cannot reproduce a constant strain field if $a_2^e \neq 0$. This conclusion, that

DOI: 10.1002/nme

blending elements cannot reproduce a constant strain field, is general and is applicable to almost all enrichment functions. It is believed that this is a cause of the loss of accuracy and decrease in convergence rate that is associated with blending; this was also argued in Chessa *et al.* [28]. The blending problem is mostly an issue for low-order elements. When higher-order shape functions are used and when the order of the shape functions that premultiply Ψ is one less than that used in the standard part of the approximation, the difficulties with blending are reduced [29, 30, 32].

Some enrichment functions, such as the step function enrichment, which appears in the original XFEM paper [2], do not have blending problems, since the enrichment terms in the blending elements are spanned by the standard finite element basis. However, in general, blending constitutes an important issue to be taken into account in the implementation of XFEM and local partition of unity methods.

3. WEIGHT FUNCTION BLENDING

In this section, we present a weight function blending for XFEM. We will consider approximations of the following form, originally proposed by Fries [35]:

$$\mathbf{u}(\mathbf{x}) = \sum_{I \in \mathcal{N}} N_I(\mathbf{x})\mathbf{u}_I + \sum_{J \in \mathcal{S}} N_J(\mathbf{x})\varphi(\mathbf{x})\mathbf{\Psi}(\mathbf{x})a_J \tag{4}$$

where $\varphi(\mathbf{x})$ is a smooth function with compact support, which we will refer to as a weight function. $N_I(\mathbf{x})$ are the finite element shape functions, $\mathbf{\Psi}(\mathbf{x})$ is the enrichment function possessing characteristics that are to be locally reproduced and a_J is the enriched degree of freedom associated with $\mathbf{\Psi}(\mathbf{x})$ and node J. The weight function is constructed so that $\varphi(\mathbf{x})>0$ only in the subdomain to be enriched; hence, node $J \in \mathcal{S}$ if there exists an $\mathbf{x} \in \text{supp}(N_J)$ such that $\varphi(\mathbf{x})>0$, where $\text{supp}(N_J)$ is the support of shape function of node J. The approximation (4) locally enriches the standard FEM approximation by $\mathbf{\Psi}(\mathbf{x})$. Locality is ensured by the compact support of $\varphi(\mathbf{x})$. We will refer to approximations of this form as weighted XFEM approximations.

We will often find it convenient to constrain all the enriched degrees of freedom to be equal, i.e. $a_I = a$; hence, we have

$$\mathbf{u}(\mathbf{x}) = \sum_{I \in \mathcal{N}} N_I(\mathbf{x})\mathbf{u}_I + \varphi(\mathbf{x})\mathbf{\Psi}(\mathbf{x})a \sum_{J \in \mathcal{S}} N_J(\mathbf{x}) \tag{5}$$

Since the partition of unity property of the shape functions is satisfied $\forall \mathbf{x} \in \text{supp}(\varphi(\mathbf{x}))$, (5) reduces to

$$\mathbf{u}(\mathbf{x}) = \sum_{I \in \mathcal{N}} N_I(\mathbf{x})\mathbf{u}_I + \varphi(\mathbf{x})\mathbf{\Psi}(\mathbf{x})a \tag{6}$$

As in the standard XFEM, we can improve the performance of the method and facilitate the application of essential boundary conditions by *shifting* the approximation. Two different shifted approximations are possible depending on how the shifts are made. The following two cases arise:

- *type 1* shifted product of the weight and enrichment function

$$\mathbf{u}(\mathbf{x}) = \sum_{I \in \mathcal{N}} N_I(\mathbf{x})\mathbf{u}_I + \sum_{J \in \mathcal{S}} N_J(\mathbf{x}) \left(\varphi(\mathbf{x})\mathbf{\Psi}(\mathbf{x}) - \varphi(\mathbf{x}_J)\mathbf{\Psi}(\mathbf{x}_J)\right) a_J \tag{7}$$

DOI: 10.1002/nme

- *type 2* shifted enrichment function (the weight is applied to the shifted enrichment function)

$$\mathbf{u}(\mathbf{x}) = \sum_{I \in \mathcal{N}} N_I(\mathbf{x})\mathbf{u}_I + \sum_{J \in \mathcal{S}} N_J(\mathbf{x})\varphi(\mathbf{x})(\boldsymbol{\Psi}(\mathbf{x}) - \boldsymbol{\Psi}(\mathbf{x}_J))a_J \tag{8}$$

When all enriched degrees of freedom are constrained to be equal at each nodes, i.e. when $a_I = a$, as in our dislocation model [16, 31], Equations (7) and (8) become

$$\mathbf{u}(\mathbf{x}) = \sum_{I \in \mathcal{N}} N_I(\mathbf{x})\mathbf{u}_I + \left(\varphi(\mathbf{x})\boldsymbol{\Psi}(\mathbf{x}) - \sum_{J \in \mathcal{S}} N_J(\mathbf{x})\varphi(\mathbf{x}_J)\boldsymbol{\Psi}(\mathbf{x}_J) \right) a \tag{9}$$

and

$$\mathbf{u}(\mathbf{x}) = \sum_{I \in \mathcal{N}} N_I(\mathbf{x})\mathbf{u}_I + \varphi(\mathbf{x}) \left(\boldsymbol{\Psi}(\mathbf{x}) - \sum_{J \in \mathcal{S}} N_J(\mathbf{x})\boldsymbol{\Psi}(\mathbf{x}_J) \right) a \tag{10}$$

respectively.

We select $\varphi(\mathbf{x})$ to be a polynomial ramp function that smoothes the transition from enriched to unenriched elements. Let Ω_e be the domain of element e. Non-enriched elements are those elements where $\varphi(\mathbf{x}) = 0$, $\forall \mathbf{x} \in \Omega_e$. An enriched element is any element where $\exists \mathbf{x} \in \Omega_e | \varphi(\mathbf{x}) \neq 0$. Let the closed set Ω^E be the enriched domain, defined as the union of all the enriched elements. Consequently, the set $\mathcal{S}$ is given by all the nodes of the enriched elements, i.e. by all the nodes in Ω^E.

The weight function is defined as $\varphi(\mathbf{x}) \in \bar{U}$, where

$$\bar{U} = \{ w(\mathbf{x}) | w(\mathbf{x}) \in C^0, w(\mathbf{x}) > 0 \ \forall \mathbf{x} \in \Omega^E \backslash \partial\Omega^E, \ w(\mathbf{x}) = 0 \ \forall \mathbf{x} \in \Omega \backslash \Omega^E \} \tag{11}$$

Displacement compatibility on the interface between enriched and unenriched subdomains is satisfied because $\varphi(\mathbf{x}) = 0, \ \forall \mathbf{x} \in \partial\Omega^E$.

The enriched domain generally consists of the union of two subdomains (Figure 3):

- the standard enrichment subdomain Ω_1^E, where $\varphi(\mathbf{x}) = 1$, $\forall \mathbf{x} \in \Omega_1^E$;
- the blending subdomain Ω_φ^E, where $0 < \varphi(\mathbf{x}) < 1$, $\forall \mathbf{x} \in \Omega_\varphi^E \backslash \partial\Omega_\varphi^E$, $\varphi(\mathbf{x}) = 0$, $\forall \mathbf{x} \in \partial\Omega^E$ and $\varphi(\mathbf{x}) = 1$, $\forall \mathbf{x} \in \partial\Omega_1^E$.

In Figure 3 we have shown Ω_φ^E as a single layer of elements. It is often desirable for Ω_φ^E to span several element layers. We note that the approximation in Ω_1^E is the same as in any fully enriched element of the standard XFEM, and hence $\boldsymbol{\Psi}$ can be reproduced exactly in Ω_1^E.

A crucial characteristic of the present technique, as in [35], is that no partially enriched elements are allowed. This ensures that the partition of unity property is satisfied in all elements.

Let Γ be a surface of discontinuity such as a crack, dislocation glide plane or material interface. Given a point $\mathbf{x} \in \Omega^E$, let $\mathrm{d} = \mathrm{d}(\mathbf{x})$ be the signed distance function from $\mathbf{x}$ to Γ.

Consider the function $\varphi(d)$ defined by

$$\varphi(d) = \begin{cases} 1, & 0 \leqslant |d| \leqslant d_i \\ (1-g)^n, & d_i < |d| < d_e \\ 0, & |d| \geqslant d_e \end{cases} \tag{12}$$

DOI: 10.1002/nme

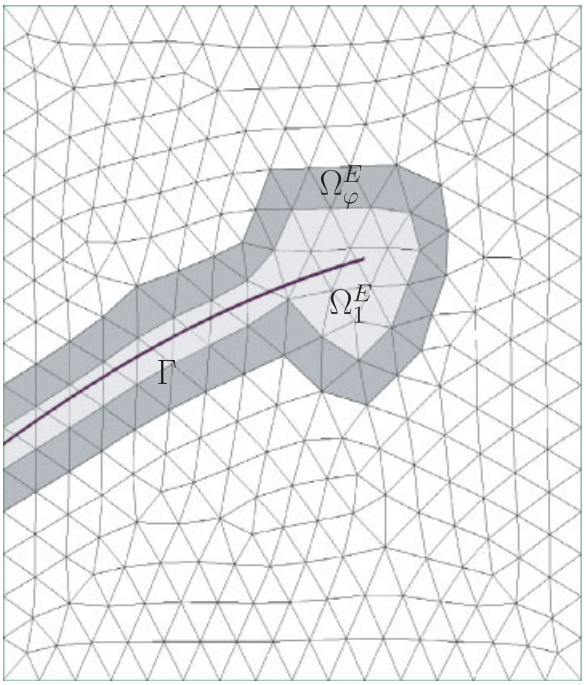

Figure 3. Decomposition of the enrichment domain Ω^E. Γ is a line of discontinuity, and the shaded area is the enriched domain Ω^E. The enriched domain is formed by a part Ω_1^E where the weight function φ has a constant plateau equal to 1 (light gray) and a part Ω_φ^E where $0 \leqslant \varphi < 1$ (dark gray).

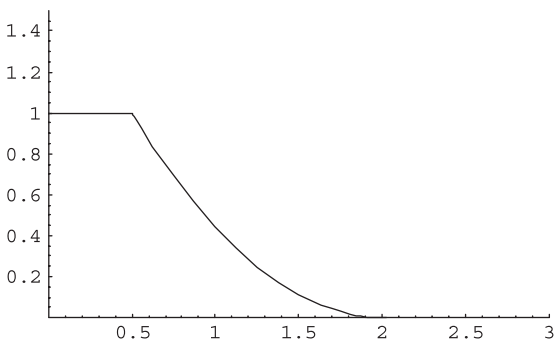

Figure 4. A sample polynomial weight function with $d_i = 0.5$, $d_e = 2$, $n = 2$.

where d_i and d_e are chosen so that $\varphi = 1$ for $|d| \leqslant d_i$ and $\varphi = 0$ for any $|d| > d_e$, n is a positive integer and g is the linear ramp function given by

$$g = \frac{|d| - d_i}{d_e - d_i} \tag{13}$$

Figure 4 illustrates a graph of φ for $n = 2$, $d_i = 0.5$ and $d_e = 2$.

DOI: 10.1002/nme

Equation (12) is inconvenient because the discontinuities in the derivatives of φ would generally lie within elements, introducing jumps in strains/stresses and complexities in the numerical evaluation of the element stiffness. A solution to this problem is to map φ to a piecewise continuous function in each finite element. This can be easily accomplished by evaluating the function at the element nodes and then interpolating the weight function by the shape functions. For this purpose, we first evaluate the function g at the nodes. Let

$$g_I = \frac{|d(\mathbf{x}_I)| - d_i}{d_e - d_i}, \quad I \in \mathcal{N} \tag{14}$$

and

$$\varphi_I = \begin{cases} 1, & g_I \leqslant 0 \\ (1-g_I)^n, & 0 < g_I < 1, \quad I \in \mathcal{N} \\ 0, & g \geqslant 1 \end{cases} \tag{15}$$

Note that the first row of the definition (15) shrinks the inner boundary of Ω_φ^E and the second row expands the outer boundary of Ω_φ^E. This is illustrated in Figure 5 with reference to a point singularity, i.e. considering the discontinuity surface Γ is collapsed to a single point. Inside the

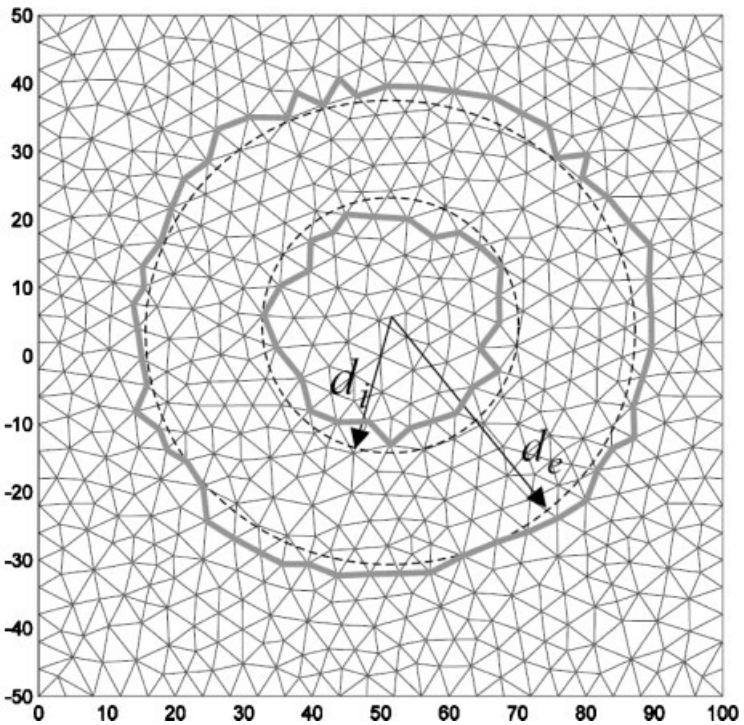

Figure 5. Weight function φ contours at 1 and 0 (thick lines) and the distances d_i and d_e from a singularity.

DOI: 10.1002/nme

elements, shape function interpolation is used, so that the weight function is given by

$$\varphi(\mathbf{x}) = \sum_{I \in \mathscr{N}} N_I(\mathbf{x}) \varphi_I, \quad \mathbf{x} \in \Omega \tag{16}$$

Finally, considering the compact support of φ, we have

$$\varphi(\mathbf{x}) = \sum_{I \in \mathscr{P}} N_I(\mathbf{x}) \varphi_I, \quad \mathbf{x} \in \Omega^E \tag{17}$$

where $\mathscr{P} \subseteq \mathscr{N}$. The function φ is everywhere continuous and differentiable and has the same polynomial order as the shape functions.

An alternative definition of the weight function for more complex enrichments is to first define the subdomain Ω_1^E where $\varphi = 1$. The distances d, d_i and d_e are then defined relative to the boundary of Ω_1^E instead of Γ. This strategy has been used in one of the examples reported in Section 8.

4. ALTERNATIVES IN SHIFTING AND A DEGENERATE CASE

Next we will study the properties of the weighted XFEM, i.e. the weighted blending, when the weight function is given by

$$\varphi(\mathbf{x}) = \sum_{J \in \mathscr{P}} N_J(\mathbf{x}), \quad \mathbf{x} \in \Omega \tag{18}$$

where $\mathscr{P}$ is the set of nodes of elements in Ω_1^E. This choice of weight function yields a method that is equivalent to that proposed in [35], where the blending layer is one element wide. We will consider the case where all enriched degrees of freedom are equal [16, 31], as we usually do for dislocation modeling, i.e. let $a_I = a$. In what follows, we will show that only the weighted XFEM with type 2 shifting, Equation (10), results in a new method. All other forms of the weighted XFEM degenerate into standard forms of XFEM.

Let

$$\mathbf{u}^{\mathrm{FE}}(\mathbf{x}) = \sum_{I \in \mathscr{N}} N_I(\mathbf{x}) \mathbf{u}_I \tag{19}$$

The standard XFEM approximation, for $a_J = a$ and for all $J \in \mathscr{Q}$, is

$$\mathbf{u}(\mathbf{x}) = \mathbf{u}^{\mathrm{FE}}(\mathbf{x}) + a\boldsymbol{\Psi}(\mathbf{x}) \sum_{J \in \mathscr{Q}} N_J(\mathbf{x}) \tag{20}$$

where $\mathscr{Q}$ is the set of enriched nodes. Similarly, from (2), the standard XFEM approximation with shifting is

$$\mathbf{u}(\mathbf{x}) = \mathbf{u}^{\mathrm{FE}}(\mathbf{x}) + a\boldsymbol{\Psi}(\mathbf{x}) \sum_{J \in \mathscr{Q}} N_J(\mathbf{x}) - a \sum_{J \in \mathscr{Q}} N_J(\mathbf{x}) \boldsymbol{\Psi}(\mathbf{x}_J) \tag{21}$$

The weighted XFEM displacement approximation obtained by substituting (18) into (6) is

$$\mathbf{u}(\mathbf{x}) = \mathbf{u}^{\mathrm{FE}}(\mathbf{x}) + a\boldsymbol{\Psi}(\mathbf{x}) \sum_{J \in \mathscr{P}} N_J(\mathbf{x}) \tag{22}$$

DOI: 10.1002/nme

The weighted XFEM approximation with type 1 shifting obtained by substituting (18) into (9) is

$$\mathbf{u}(\mathbf{x}) = \mathbf{u}^{\mathrm{FE}}(\mathbf{x}) + a\boldsymbol{\Psi}(\mathbf{x}) \sum_{J \in \mathscr{P}} N_J(\mathbf{x}) - a \sum_{J \in \mathscr{P}} N_J(\mathbf{x}) \boldsymbol{\Psi}(\mathbf{x}_J) \tag{23}$$

The weighted XFEM approximation with type 2 shifting obtained by substituting (18) into (10) is

$$\mathbf{u}(\mathbf{x}) = \mathbf{u}^{\mathrm{FE}}(\mathbf{x}) + a\boldsymbol{\Psi}(\mathbf{x}) \sum_{J \in \mathscr{P}} N_J(\mathbf{x}) - a \sum_{J \in P} N_J(\mathbf{x}) \sum_{K \in \mathscr{S}} N_K(\mathbf{x}) \boldsymbol{\Psi}(\mathbf{x}_K) \tag{24}$$

From (20)–(24) we can make the following observations:

1. The weighted XFEM displacement approximation (22) without shifting is equivalent to the standard XFEM approximation (20) when $\mathscr{Q} \equiv \mathscr{P}$. Hence, approximation (22) will not improve the accuracy or the convergence rate.
2. The weighted XFEM displacement approximation with type 1 shifting (23) is equivalent to the standard XFEM approximation with shifting (21) when $\mathscr{Q} \equiv \mathscr{P}$. Hence, approximation (23) will not improve the accuracy or the convergence rate of the XFEM.
3. The basis functions in (20) and (21) are identical; hence, approximations (20)–(23) will yield the same results when $\mathscr{Q} \equiv \mathscr{P}$. This has been verified numerically.
4. Of all the approximations considered, only (24) is different from the standard XFEM approximation. Numerical studies have shown that approximation (24) yields improved accuracy and optimum convergence rates.

5. DISLOCATION AND CRACK ENRICHMENTS

In this section, various local enrichment approximations for crack and dislocation problems are given. These two problems will be examined together as they are very similar.

5.1. Dislocation enrichment

The enriched displacement degrees of freedom are equal; hence, we adopt a weighted approximation of the form (24), i.e. that with type 2 shifting. The approximation is

$$\mathbf{u}(\mathbf{x}) = \mathbf{u}^{\mathrm{FE}}(\mathbf{x}) + \mathbf{b}\bar{\varphi}(\mathbf{x}) \left[H(y) - \sum_{J \in \mathscr{S}^{\mathscr{H}}} N_J(\mathbf{x}) H_J \right] + b\varphi(\mathbf{x}) \left[\mathbf{u}_D^{\infty}(\mathbf{x}) - \sum_{K \in \mathscr{S}^{\infty}} N_K(\mathbf{x}) \mathbf{u}_{D_K}^{\infty} \right] \tag{25}$$

where $\mathbf{x} = (x, y)$, $H(\cdot)$ is the Heaviside step function, $H_J = H(y_J)$, $\mathscr{S}^{\mathscr{H}}$ is the set of Heaviside step function enriched nodes (a node $J \in \mathscr{S}^{\mathscr{H}}$ if there exists $\mathbf{x} \in \mathrm{supp}(N_J)$ such that $\bar{\varphi}(\mathbf{x}) > 0$), $\mathscr{S}^{\infty}$ is the set of singular or analytically enriched nodes (a node $J \in \mathscr{S}^{\infty}$ if there exists $\mathbf{x} \in \mathrm{supp}(N_J)$ such that $\varphi(\mathbf{x}) > 0$) and $\mathbf{b}$ is the Burgers vector. Moreover, two different weight functions have been introduced in (25). They are both approximated by shape functions with the same mesh; hence,

$$\bar{\varphi}(\mathbf{x}) = \sum_{J \in \mathscr{P}^{\mathscr{H}}} N_J(\mathbf{x}) \bar{\varphi}_J \tag{26}$$

DOI: 10.1002/nme

and

$$\varphi(\mathbf{x}) = \sum_{K \in \mathscr{P}^{\infty}} N_K(\mathbf{x}) \varphi_K \tag{27}$$

For an edge dislocation, the enrichment is the plane strain solution in an infinite domain with the core located at $(0,0)$ and glide plane extending along the negative x-axis; it is given by

$$\mathbf{u}_D^{\infty}(x,y) = \begin{bmatrix} \dfrac{x\,y}{4\pi(x^2+y^2)(1+\nu)} + \dfrac{\arctan(x,y)}{2\pi} \\ \dfrac{-x^2}{4\pi(x^2+y^2)(1-\nu)} - \dfrac{(1-2\nu)\log(\sqrt{x^2+y^2})}{4\pi(1-\nu)} \end{bmatrix} \tag{28}$$

where ν is Poisson's ratio and $\mathbf{u}_{D_K}^{\infty} = \mathbf{u}_D^{\infty}(x_K, y_K)$. For (25) to be general, transformations of the reference system are applied to the enrichment function (28); see [16, 41] for more details.

We will consider three different enrichment schemes, i.e. three different choices for $\mathscr{S}^{\mathscr{H}}$, $\mathscr{S}^{\infty}$, φ and $\bar{\varphi}$.

1. Singular enrichment without Heaviside enrichment and with a fixed enrichment radius (EEL): In this scheme, $\mathscr{S}^{\mathscr{H}}$ is the null set. $\mathscr{S}^{\infty}$ is the set of nodes within a given number of element layers from the glide plane or core, as shown in Figure 6(a). φ is defined by (17), where d_i and d_e are defined to be constant distances from the glide plane, as shown in Figure 13(a). We label this enrichment EEL because it corresponds to the enriched element layers scheme used in [8] with the standard XFEM.
2. Singular enrichment without Heaviside enrichment and with a variable enrichment radius (DOL): In this scheme $\mathscr{S}^{\mathscr{H}}$ is the null set. $\mathscr{S}^{\infty}$ is defined as the set of nodes within a given number of element layers from the core and by the nodes of all elements within one element layer from the glide plane, as shown in Figure 6(c). $\varphi_I = 1$ for all nodes of elements cut by the glide plane; at all other nodes, φ_I is defined by (15) and (17) with distances d_i and d_e measure relative to the dislocation core. This weight function is shown in Figure 13(b). We label this enrichment DOL because it corresponds to the dislocation origin and layers scheme used in [8] with the standard XFEM, which is shown in Figure 6(b).
3. A combination of singular enrichment and Heaviside enrichment (DOL+H): This scheme is similar to DOL except that slip away from the core is modeled by the tangential jump enrichment and not the singular enrichment. $\mathscr{S}^{\infty}$ is the set of nodes within a given number of layers from the core and $\mathscr{S}^{\mathscr{H}}$ is the set of nodes far from the core with supports cut by the glide plane, as shown in Figure 6(d). φ_I is defined by (17) with distances d_i and d_e measure relative to the dislocation core, as shown in Figure 14(a) and $\bar{\varphi}_I = 1 - \varphi_I$. We will elaborate on these definitions in Section 6.

Finally, we would like to point out that in continuum dislocation modeling, the Burgers vector is known. Hence, the contribution from the enrichment part of the displacement approximation appears in the discrete equations as a vector of nodal forces, see [16, 31, 41] for more details.

DOI: 10.1002/nme

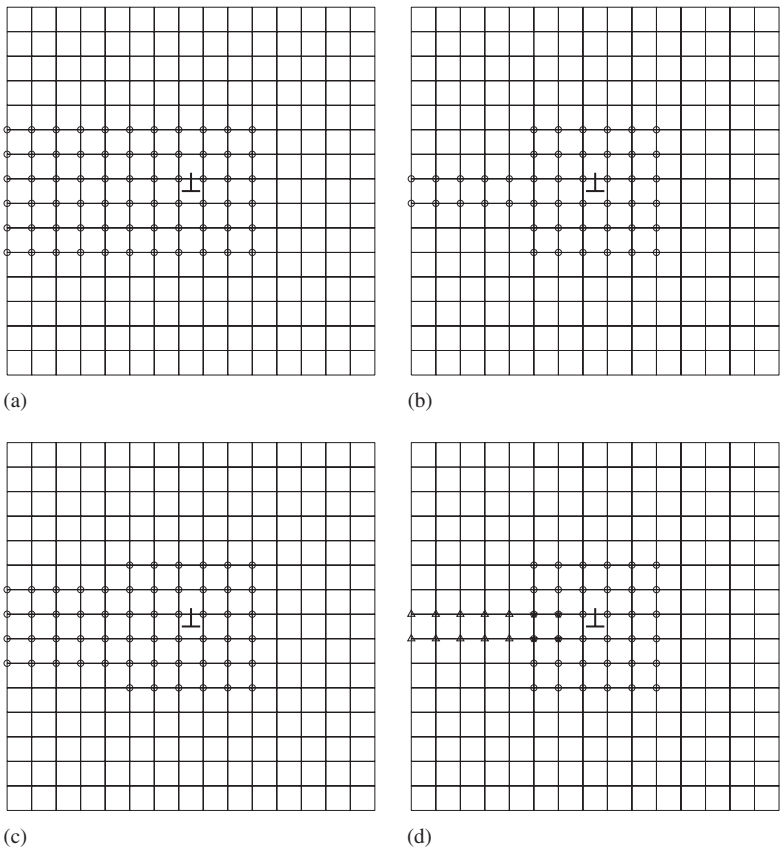

Figure 6. Enriched nodes for the considered enrichment schemes. Circles denote nodes enriched by the singular analytical enrichment function and triangles denote nodes enriched by the Heaviside step function: (a) EEL; (b) DOL for the standard XFEM; (c) DOL for the weighted XFEM; and (d) DOL+H.

5.2. *Crack enrichment*

The displacement approximation for a mode I crack studied here was first proposed in [40]. As in [40] we will constrain all of the enriched degrees of freedom associated with the crack tip enrichment to be equal. Therefore, we will again adopt an approximation with type 2 shifting. The approximation for a mode I crack is

$$\mathbf{u}(\mathbf{x}) = \mathbf{u}^{\mathrm{FE}}(\mathbf{x}) + \bar{\varphi}(\mathbf{x}) \sum_{J \in \mathscr{S}^{\mathscr{H}}} N_J(\mathbf{x})[H(y) - H_J]a_J + K_I \varphi(\mathbf{x}) \left[\mathbf{u}^{\infty}_{K_I}(\mathbf{x}) - \sum_{L \in \mathscr{S}^{\infty}} N_L(\mathbf{x}) \mathbf{u}^{\infty}_{K_I, L} \right] \quad (29)$$

where a_J is the enriched degree of freedom associated with the Heaviside step enrichment and node J, K_I is the enriched degree of freedom associated with the analytical asymptotic solution $\mathbf{u}^{\infty}_{K_I}(\mathbf{x})$ and corresponds to the mode I stress intensity factor. $\mathbf{u}^{\infty}_{K_I}(\mathbf{x})$ is the first term of the analytic asymptotic crack tip displacement field for a mode I crack with unit stress intensity factor and is

DOI: 10.1002/nme

given by

$$\mathbf{u}_{K_I}^{\infty}=\frac{\sqrt{r}}{2\sqrt{2\pi}\mu}\begin{bmatrix}\left(-\left(\frac{1}{2}\right)+\kappa\right)\cos\left(\frac{\theta}{2}\right)-\frac{\cos(3\theta/2)}{2}\\ \left(\frac{1}{2}+\kappa\right)\sin\left(\frac{\theta}{2}\right)-\frac{\sin(3\theta/2)}{2}\end{bmatrix} \tag{30}$$

where r and θ are polar coordinates defined relative to the crack tip, μ is the shear modulus of the material and $\kappa=3-4\nu$ for plain strain and $\mathbf{u}_{K_I,L}^{\infty}=\mathbf{u}_{K_I}^{\infty}(x_L, y_L)$. For the enrichment of an arbitrary oriented crack see [40]. The weight functions $\bar{\varphi}(\mathbf{x})$ and $\varphi(\mathbf{x})$ are interpolated by (26) and (27), respectively. Again, the definition of $\mathscr{S}^{\mathscr{H}}$ and $\mathscr{S}^{\infty}$ will depend on which of the enrichment schemes (EEL, DOL or DOL+H) is adopted.

The third term in (29), the singular enrichment, is identical to the form proposed in Gifford and Hilton [37], except for the weight $\varphi(\mathbf{x})$. They mention a weighting of the enrichment, but note that it is not needed, which is probably due to their use of higher-order elements; see Legay *et al.* [30]. They did not include the step enrichment; hence, the crack had to be aligned with the element edges.

6. MERGING ANALYTIC AND HEAVISIDE ENRICHMENTS

The DOL+H enrichment scheme is the most effective in the modeling of cracks and dislocations. It combines analytic singular enrichment around the crack tip (or dislocation core) with the Heaviside step enrichment along the crack faces (or glide plane). This combined enrichment scheme introduces three different blending domains in the standard XFEM. The first is the blending between the Heaviside step enriched domain and the unenriched domain; this blending does not generate any blending problems because the enrichment vanishes at the outside edges of the enriched elements. The second is the blending between the singular enriched domain and the unenriched domain; here the difficulties with blending can be solved using the strategy described above. The third is the blending between the Heaviside step enriched domain and the singular enriched domain, which is the focus of this section.

We will restrict our discussion to the edge dislocation problem for clarity. In this case there is a constant displacement discontinuity across the glide plane. The selection of an effective merging strategy involves the judicious choice of $\bar{\varphi}_I$, φ_I, $\mathscr{P}^{\mathscr{H}}$ and $\mathscr{P}^{\infty}$ in Equations (26) and (27). The two weight functions can be chosen independently everywhere expect for the elements cut by the glide plane. In dislocation problems, for the displacement field to be compatible, the tangential displacement discontinuity must be equal to the Burgers vector along the glide plane; hence, when $\varphi<1$, the Heaviside enrichment has to compensate for this effect. Hence, we will require that $\bar{\varphi}=1-\varphi$ in all elements cut by the glide plane. In this manner the correct displacement discontinuity is recovered. A similar approach can be employed for cracks. This procedure is illustrated by a schematic in Figure 7. In the singular enriched subdomain, the weight for the singular enrichment is $\varphi=1$; in the step function enriched subdomain, the weight for the singular enrichment step function is $\bar{\varphi}=1$ and in the transition subdomain, where both enrichments are applied, $\varphi+\bar{\varphi}=1$. We have shown a linear transition of the weight functions, as in Figure 7, but other approaches such as splines can also be used. Note that the computation of the weighting function of the Heaviside step function enrichment is needed only in the subdomain where the

DOI: 10.1002/nme

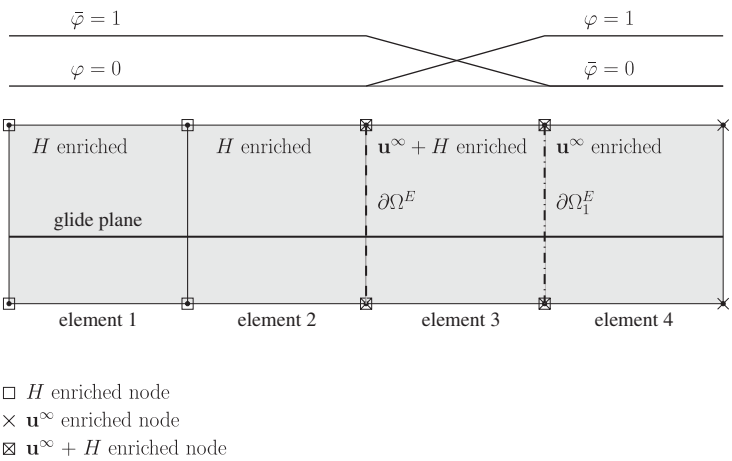

Figure 7. A one-dimensional depiction of the merging of Heaviside and analytic enrichments. Mixed enrichment elements and a second weight function $\bar{\varphi}$ ensure a correct displacement field.

singular and Heaviside enrichments merge, i.e. in the $\mathbf{u}^\infty+H$ enriched subdomain. In contrast to the standard XFEM, the Heaviside function enrichment domain overlaps the asymptotic solution enrichment domain. This has been found to be very beneficial; otherwise stress oscillations will occur between the asymptotic solution enrichment domain and the Heaviside function enrichment domain.

7. BOUNDARY INTEGRATION

The integration of enrichment functions with strong singularities, such as the edge dislocation enrichment (25) or the mode I crack enrichment (29), is computationally expensive because of the large number of Gauss points required for an accurate evaluation of the element stiffness [16]. Here we develop, for linear problems with shifted enrichments, an extension of the basic method proposed in [16], which simplifies the integration by the transformation of domain integrals to equivalent contour integrals.

Several additional terms appear in the expression of the element stiffness when the enrichment is shifted. The method is applicable only to elements for which all nodes of the element are enriched and for which all enriched degrees of freedom at all nodes of the element are equal. In addition, the enrichment function must be self-equilibrated, similar to those of the edge dislocation enrichment (25) and the crack enrichment (29), although the method works reasonably well for the other singular enrichments used in XFEM.

Let $\boldsymbol{\nabla}$ be the del differential operator and $\boldsymbol{\nabla}^{\mathrm{s}}$ be the symmetric gradient operator so that the strain displacement equation is $\boldsymbol{\varepsilon}=\boldsymbol{\nabla}^{\mathrm{s}}\mathbf{u}=\frac{1}{2}(\boldsymbol{\nabla}^{\top}\mathbf{u}+\boldsymbol{\nabla}\mathbf{u})$ and the equilibrium equation is $\boldsymbol{\nabla}\cdot\boldsymbol{\sigma}+\mathbf{g}=\mathbf{0}$, where $\mathbf{g}$ are the body forces. The Cauchy stress, $\boldsymbol{\sigma}$, is given by $\boldsymbol{\sigma}=\mathbf{C}\boldsymbol{\varepsilon}$ and $\mathbf{C}$ is the Hookean tensor. Moreover, let

$$\langle\delta\boldsymbol{\varepsilon},\boldsymbol{\sigma}\rangle=\int_{\Omega_e}\delta\boldsymbol{\varepsilon}:\boldsymbol{\sigma}\,\mathrm{d}\Omega,\quad [\delta\mathbf{v},\mathbf{w}]=\int_{\partial\Omega_e}\delta\mathbf{v}\cdot\mathbf{w}\,\mathrm{d}A \tag{31}$$

DOI: 10.1002/nme

where the variation δ applies to a test function. The principle of virtual work for a single finite element in the absence of body forces gives

$$\langle \delta\boldsymbol{\varepsilon}, \boldsymbol{\sigma}\rangle - \delta\mathbf{u}\cdot\mathbf{f} = \mathbf{0} \tag{32}$$

where $\mathbf{f}$ are the equivalent nodal forces.

We will consider displacement approximations of the form (2) and (10) with $\varphi = 1$ and the constraint that $a_I = a$; hence, we have

$$\mathbf{u} = \mathbf{N}\mathbf{d} + (\boldsymbol{\Psi} - \boldsymbol{\Psi}^\star)a \tag{33}$$

where

$$\boldsymbol{\Psi}^\star(\mathbf{x}) = \sum_{I=1}^{n} N_I(\mathbf{x})\boldsymbol{\Psi}(\mathbf{x}_I) \tag{34}$$

in which n is the number of nodes, $\mathbf{d} = \{\mathbf{u}_1, \ldots, \mathbf{u}_n\}$ and $\mathbf{N}$ collects the shape functions for all the nodes and displacement components.

From the strain–displacement equation and (33), the strain is given by

$$\boldsymbol{\varepsilon} = \nabla^{\mathrm{s}}\mathbf{N}\mathbf{d} + \nabla^{\mathrm{s}}\left(\boldsymbol{\Psi} - \boldsymbol{\Psi}^\star\right)a = \mathbf{B}\mathbf{d} + a\boldsymbol{\varepsilon}^\infty - a\boldsymbol{\varepsilon}^\star \tag{35}$$

where

$$\mathbf{B} = \nabla^{\mathrm{s}}\mathbf{N} \tag{36a}$$

$$\boldsymbol{\varepsilon}^\infty = \nabla^{\mathrm{s}}\boldsymbol{\Psi} \tag{36b}$$

$$\boldsymbol{\varepsilon}^\star = \nabla^{\mathrm{s}}\boldsymbol{\Psi}^\star \tag{36c}$$

The stress is given by

$$\boldsymbol{\sigma} = \mathbf{C}\mathbf{B}\mathbf{d} + a\boldsymbol{\sigma}^\infty - a\boldsymbol{\sigma}^\star \tag{37}$$

where

$$\boldsymbol{\sigma}^\infty = \mathbf{C}\boldsymbol{\varepsilon}^\infty \tag{38a}$$

$$\boldsymbol{\sigma}^\star = \mathbf{C}\boldsymbol{\varepsilon}^\star \tag{38b}$$

Substitution of (33), (35) and (37) into (32) gives

$$\delta\mathbf{d}^\top(\langle \mathbf{B}, \mathbf{C}\mathbf{B}\rangle\mathbf{d} + \langle \mathbf{B}, \mathbf{C}\boldsymbol{\varepsilon}^\infty\rangle a - \langle \mathbf{B}, \mathbf{C}\boldsymbol{\varepsilon}^\star\rangle a) = \delta\mathbf{d}^\top\mathbf{f}_d \tag{39}$$

and

$$\begin{aligned}&\delta a(\langle \boldsymbol{\varepsilon}^\infty, \mathbf{C}\mathbf{B}\rangle - \langle \boldsymbol{\varepsilon}^\star, \mathbf{C}\mathbf{B}\rangle)\mathbf{d} - \delta a(\langle \boldsymbol{\varepsilon}^\infty, \mathbf{C}\boldsymbol{\varepsilon}^\star\rangle + \langle \boldsymbol{\varepsilon}^\star, \mathbf{C}\boldsymbol{\varepsilon}^\infty\rangle)a\\ &+\delta a(\langle \boldsymbol{\varepsilon}^\star, \mathbf{C}\boldsymbol{\varepsilon}^\star\rangle + \langle \boldsymbol{\varepsilon}^\infty, \mathbf{C}\boldsymbol{\varepsilon}^\infty\rangle)a = \delta a f_a\end{aligned} \tag{40}$$

DOI: 10.1002/nme

Invoking the arbitrariness of $\delta\mathbf{d}$ and δa, we obtain the following system of equations:

$$\langle \mathbf{B}, \mathbf{CB}\rangle \mathbf{d} + \langle \mathbf{B}, \mathbf{C}\boldsymbol{\varepsilon}^{\infty}\rangle a - \langle \mathbf{B}, \mathbf{C}\boldsymbol{\varepsilon}^{\star}\rangle a = \mathbf{f}_d \tag{41}$$

$$\begin{aligned}&(\langle \boldsymbol{\varepsilon}^{\infty}, \mathbf{CB}\rangle - \langle \boldsymbol{\varepsilon}^{\star}, \mathbf{CB}\rangle)\mathbf{d} - (\langle \boldsymbol{\varepsilon}^{\infty}, \mathbf{C}\boldsymbol{\varepsilon}^{\star}\rangle + \langle \boldsymbol{\varepsilon}^{\star}, \mathbf{C}\boldsymbol{\varepsilon}^{\infty}\rangle)a \\ &+ (\langle \boldsymbol{\varepsilon}^{\star}, \mathbf{C}\boldsymbol{\varepsilon}^{\star}\rangle + \langle \boldsymbol{\varepsilon}^{\infty}, \mathbf{C}\boldsymbol{\varepsilon}^{\infty}\rangle)a = f_a\end{aligned} \tag{42}$$

Equations (41) and (42) can be written in matrix form as

$$\begin{bmatrix} \mathbf{K}_{dd} & \mathbf{K}_{da} \\ \mathbf{K}_{da}^{\top} & K_{aa} \end{bmatrix} \begin{Bmatrix} \mathbf{d} \\ a \end{Bmatrix} + \begin{bmatrix} \mathbf{0} & \mathbf{K}_{da}^{\star} \\ \mathbf{K}_{da}^{\star\top} & K_{aa}^{\star} \end{bmatrix} \begin{Bmatrix} \mathbf{d} \\ a \end{Bmatrix} = \begin{Bmatrix} \mathbf{f}_d \\ f_a \end{Bmatrix} \tag{43}$$

The second matrix product contains the terms that only appear when shifting is used. The submatrices are given by

$$\mathbf{K}_{dd} = \langle \mathbf{B}, \mathbf{CB}\rangle \tag{44a}$$

$$\mathbf{K}_{da} = \langle \mathbf{B}, \boldsymbol{\sigma}^{\infty}\rangle \tag{44b}$$

$$K_{aa} = \langle \boldsymbol{\varepsilon}^{\infty}, \boldsymbol{\sigma}^{\infty}\rangle \tag{44c}$$

$$\mathbf{K}_{da}^{\star} = -\langle \mathbf{B}, \boldsymbol{\sigma}^{\star}\rangle \tag{44d}$$

$$K_{aa}^{\star} = \langle \boldsymbol{\varepsilon}^{\star}, \boldsymbol{\sigma}^{\star}\rangle - \langle \boldsymbol{\varepsilon}^{\infty}, \boldsymbol{\sigma}^{\star}\rangle - \langle \boldsymbol{\varepsilon}^{\star}, \boldsymbol{\sigma}^{\infty}\rangle \tag{44e}$$

The numerical integration of (44b), (44c) and (44e) when $\boldsymbol{\Psi}$ is singular is computationally expensive. We propose the following transformation to alleviate this problem. Consider the domain integral (44c) which, using the definitions (31) and (36b), can be written as

$$K_{aa} = \int_{\Omega_e} \boldsymbol{\nabla}^{\mathrm{s}} \boldsymbol{\Psi} : \boldsymbol{\sigma}^{\infty} \, \mathrm{d}\Omega \tag{45}$$

Applying integration by parts and the divergence theorem gives

$$\begin{aligned} K_{aa} &= \int_{\partial\Omega_e} \boldsymbol{\Psi} \cdot \boldsymbol{\sigma}^{\infty} \mathbf{n} \, \mathrm{d}A - \int_{\Omega_e} \boldsymbol{\Psi} \cdot \boldsymbol{\nabla} \cdot \boldsymbol{\sigma}^{\infty} \, \mathrm{d}\Omega \\ &= \int_{\partial\Omega_e} \boldsymbol{\Psi} \cdot \boldsymbol{\sigma}^{\infty} \mathbf{n} \, \mathrm{d}A \end{aligned} \tag{46}$$

where $\mathbf{n}$ is the outward normal to $\partial\Omega_e$ and the last step follows from the equilibrium of $\boldsymbol{\sigma}^{\infty}$.

Applying similar transformations to (44b) and (44e) we have

$$\mathbf{K}_{da} = [\mathbf{N}, \boldsymbol{\sigma}^{\infty}\mathbf{n}] \tag{47a}$$

$$K_{aa}^{\star} = \langle \boldsymbol{\varepsilon}^{\star}, \boldsymbol{\sigma}^{\star}\rangle - 2[\boldsymbol{\Psi}^{\star}, \boldsymbol{\sigma}^{\infty}\mathbf{n}] \tag{47b}$$

DOI: 10.1002/nme

where we have used the identity $\langle \boldsymbol{\varepsilon}^{\infty}, \boldsymbol{\sigma}^{\star} \rangle^{\top} = \langle \boldsymbol{\varepsilon}^{\infty}, \boldsymbol{\sigma}^{\star} \rangle = \langle \boldsymbol{\varepsilon}^{\star}, \boldsymbol{\sigma}^{\infty} \rangle$. In integral form the terms of the stiffness matrix are

$$\mathbf{K}_{dd} = \int_{\Omega_E} \mathbf{B}^{\top} \mathbf{C} \mathbf{B} \, \mathrm{d}\Omega \tag{48a}$$

$$\mathbf{K}_{da} = \int_{\Omega_E} \mathbf{B}^{\top} \boldsymbol{\sigma}^{\infty} \, \mathrm{d}\Omega = \int_{\partial\Omega_e} \mathbf{N}^{\top} \boldsymbol{\sigma}^{\infty} \mathbf{n} \, \mathrm{d}A \tag{48b}$$

$$K_{aa} = \int_{\Omega_E} \varepsilon^{\infty} : \boldsymbol{\sigma}^{\infty} \, \mathrm{d}\Omega = \int_{\partial\Omega_e} \boldsymbol{\Psi} \cdot \boldsymbol{\sigma}^{\infty} \mathbf{n} \, \mathrm{d}A \tag{48c}$$

$$\mathbf{K}^{\star}_{da} = -\int_{\Omega_E} \mathbf{B}^{\top} \boldsymbol{\sigma}^{\star} \, \mathrm{d}\Omega \tag{48d}$$

$$K^{\star}_{aa} = \int_{\Omega_E} \boldsymbol{\varepsilon}^{\star} : \boldsymbol{\sigma}^{\star} \, \mathrm{d}\Omega - 2 \int_{\Omega_E} \boldsymbol{\varepsilon}^{\infty} : \boldsymbol{\sigma}^{\star} \, \mathrm{d}\Omega \tag{48e}$$

$$= \int_{\Omega_E} \boldsymbol{\varepsilon}^{\star} : \boldsymbol{\sigma}^{\star} \, \mathrm{d}\Omega - 2 \int_{\partial\Omega_e} \boldsymbol{\Psi}^{\star} \cdot \boldsymbol{\sigma}^{\infty} \mathbf{n} \, \mathrm{d}A \tag{48f}$$

The steps leading to Equations (48) depend on the additive decomposition of the stress (37), which is a result of the linearity of the strain–displacement equation (35) and the constitutive relation (37)–(38). For nonlinear problems, the stress cannot be additively decomposed and hence Equations (37) and (48) do not hold.

The proposed boundary integration scheme is compared with the sub-cell integration method [2], and the nearly polar integration method [36, 38]. Figure 8 illustrates these three different methods.

We compare the efficiency of these integration schemes by comparing the L2 norm of the XFEM solutions for various numbers of quadrature points for the dislocation problem described in the following section. We normalize the L2 norm by the magnitude of the Burgers vector. Figure 9 reports the accuracy of the XFEM solution for each of the three schemes for various numbers of quadrature points. It can be seen that both the boundary and the nearly polar methods are much more accurate than the sub-cell method. It may also be observed that the boundary integration

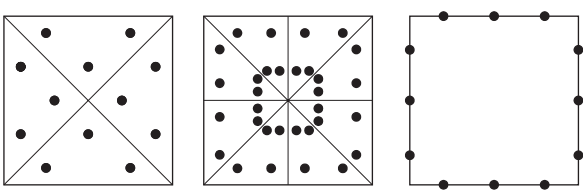

Figure 8. Location of the quadrature points from various integration schemes for the crack tip or dislocation core element. (a) The sub-cell method with four sub-cells and a second-order triangular quadrature rule. (b) The nearly polar integration method with eight subdomains and a mapped second-order bi-unit square quadrature rule. (c) The boundary integration method with a fifth-order quadrature rule along each edge.

DOI: 10.1002/nme

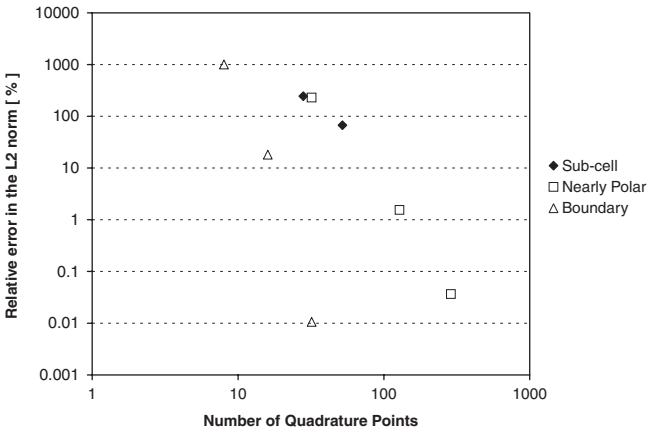

Figure 9. Comparison of the accuracy of the boundary integration method, the sub-cell quadrature method and the nearly polar integration method.

scheme requires only 32 quadrature points and that the nearly polar scheme requires, for the same accuracy, about 10 times more quadrature points. The convergence rate of the boundary integration scheme with increasing the number of quadrature points appears to be higher than that of the nearly polar scheme. We have used the boundary integration scheme with 32 quadrature points in all of the computations reported in this paper.

8. NUMERICAL EXAMPLES

8.1. Edge dislocation problem

Consider a square plate with sides of length $10\,\mu\text{m}$, Young's modulus $E=0.12141\,\text{N}\,\mu\text{m}^{-2}$ and Poisson's ratio $v=0.34$. The origin of the coordinate system is located at the center of the plate. The plate contains a single dislocation with core located at the origin, glide plane extending along the negative x-axis, Burgers vector $b=0.000255\,\mu\text{m}$ and the core of radius $0.001\,\mu\text{m}$ is removed from the domain. To reproduce the infinite medium results, the linear elastic stresses σ_D^{∞} are computed from (28) and the corresponding traction is applied along the boundary on the plate. The plate is constrained to eliminate rigid body motions.

We will adopt approximation (25) with four-node bilinear elements and enrich the domain according to the schemes *EEL*, *DOL* and *DOL*+*H*.

A study of the properties of the proposed method has been carried out considering the following combinations of parameters of a mesh of 25×25 elements:

- 4, 6 and 8 enrichment layers;
- weight function exponents $n=2, 4, 6$;
- the constant plateau distance d_i has been defined to contain 2, 3 or n_l-1 layers of elements, where n_l is the number of enrichment layers.

The relative error in energy to the analytic solution [42] has then been evaluated for each of the three enrichment schemes EEL, DOL, DOL+H and is reported in Figures 10–12, respectively.

DOI: 10.1002/nme

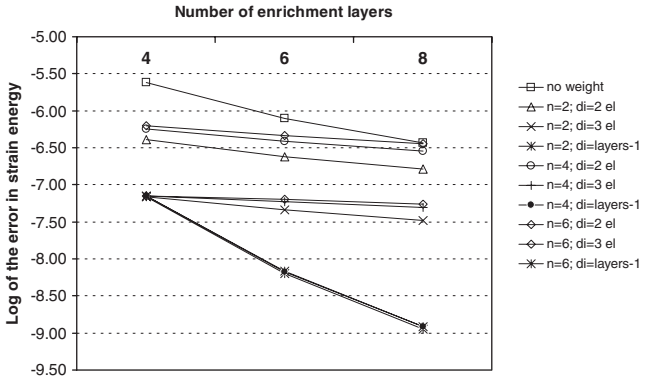

Figure 10. Relative error in energy by varying the ramp exponent n (Equation (12)), the number of enrichment layers and the size of the constant plateau (enrichment-type EEL); 'no weight' corresponds to the standard XFEM.

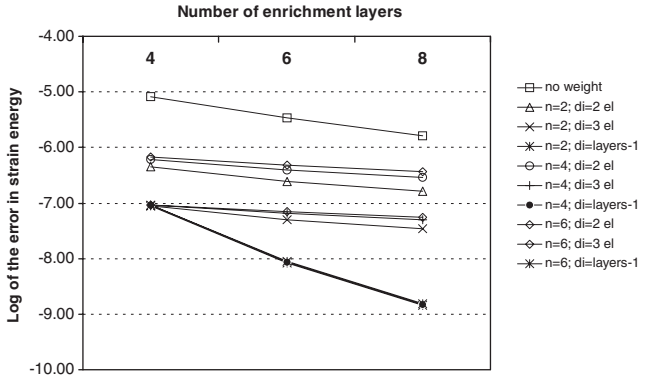

Figure 11. Relative error in energy by varying the ramp exponent n (Equation (12)), the number of enrichment layers and the size of the constant plateau (enrichment-type DOL); 'no weight' corresponds to the standard XFEM.

In all cases there is a significant reduction in the error when compared with the standard XFEM, which is labeled *no weight*.

The exponent n of the ramp plays almost no role, so that it may be convenient to choose it as low as possible. Since the weight function is always bilinear inside the elements because of the shape function interpolation, using a higher exponent n does not require any changes in the quadrature of the element stiffness.

In all the examined enrichments there is a common trend: the error always decreases with increasing d_i, decreasing the ramp exponent n and increasing the number of enriched layers. The results of the EEL scheme are slightly more accurate than those of the other schemes; however, its additional computational cost makes the DOL and DOL+H schemes more efficient.

Figure 13 reports typical contours of the weight function and the computed shear stress for the two enrichments techniques EEL and DOL with 6 layers of enrichment and a constant unit weight

DOI: 10.1002/nme

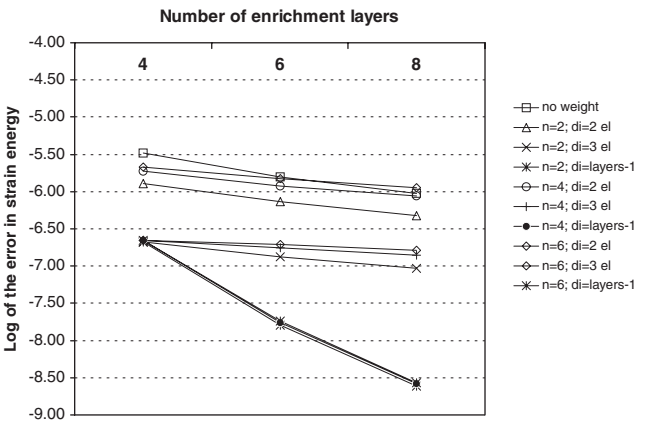

Figure 12. Relative error in energy by varying the ramp exponent n (Equation (12)), the number of enrichment layers and the size of the constant plateau (enrichment-type DOL+H); 'no weight' corresponds to the standard XFEM.

function plateau of three layers. The stress is plotted, as common practice in finite elements, by averaging the nodal values of the contiguous elements. In Figure 13(c) and (d), the solutions from the standard XFEM are shown; the parasitic stress oscillations at the boundary of the enrichment subdomain are quite evident. In Figure 13(e) and (f) the results from the proposed blending method are shown. Here we see that the oscillations in the stress contours have been eliminated. The stress contours for the DOL+H enrichment scheme are shown in Figure 14. Here again we can see that there are no parasitic oscillations in the stress contours.

Finally, the dependence of the error on the mesh size has been computed to evaluate the convergence rates. Meshes from 5×5 to 135×135 elements, with an enrichment area of constant size [16], have been solved. Results are reported in Figure 15, where a very significant improvement with all of the enrichment schemes is apparent. Table I reports the convergence rates of the three examined enrichment schemes. In all cases, the weighted XFEM improves the convergence rate of XFEM by more than a factor of two. In fact, the convergence rate for the weighted XFEM is optimal.

These results suggest that the optimal choice of the weight function for the singular-analytical enrichment for a given number of enriched layers is

$$\varphi(\mathbf{x})=\sum_{K\in\mathscr{P}^{\infty}} N_K(\mathbf{x}) \tag{49}$$

which is the same weight function proposed in Fries [35]. We note that this weight function must be coupled with type 2 shifting to obtain improved results, as discussed in Section 4.

8.2. *Mode I crack*

Consider an edge crack in a square plate. The geometric and material data of the previous example are used, replacing the glide plane with the crack and the dislocation core with the crack tip. The traction $\mathbf{n}\cdot\boldsymbol{\sigma}^{\infty}_{K_I}$ is applied on the boundary and rigid body motion is constrained. We used a

DOI: 10.1002/nme

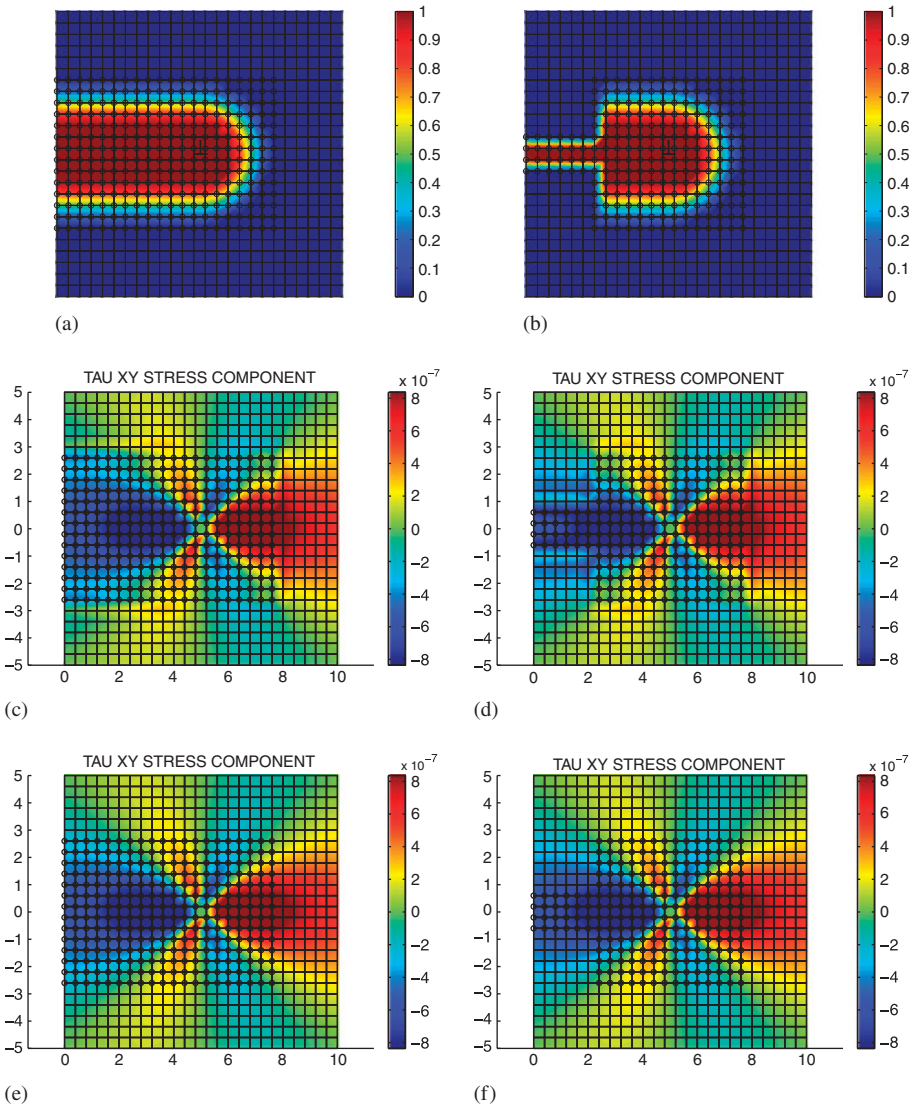

Figure 13. Results and weight functions for the dislocation problem. Enrichment-type EEL on the left column and enrichment-type DOL on the right column. From top to bottom (a,b) weight function; (c,d) standard enrichment (no weight function used); and (e,f) proposed weighted enrichment with $n=1$, a constant plateau of 3 layers of elements and a total of 6 enrichment layers.

structured mesh of bilinear elements and the displacement approximation (29). We will compare the results from the DOL and DOL+H enrichment strategies.

To illustrate qualitatively the effectiveness of the proposed blending method, Figure 16 shows the computed $\boldsymbol{\sigma}_y$ and $\boldsymbol{\sigma}_x$ stresses for a 25×25 element mesh and the DOL+H enrichment scheme. In the two layers of nodes around the crack tip, the enrichment of Liu *et al.* [40] and a linear

DOI: 10.1002/nme

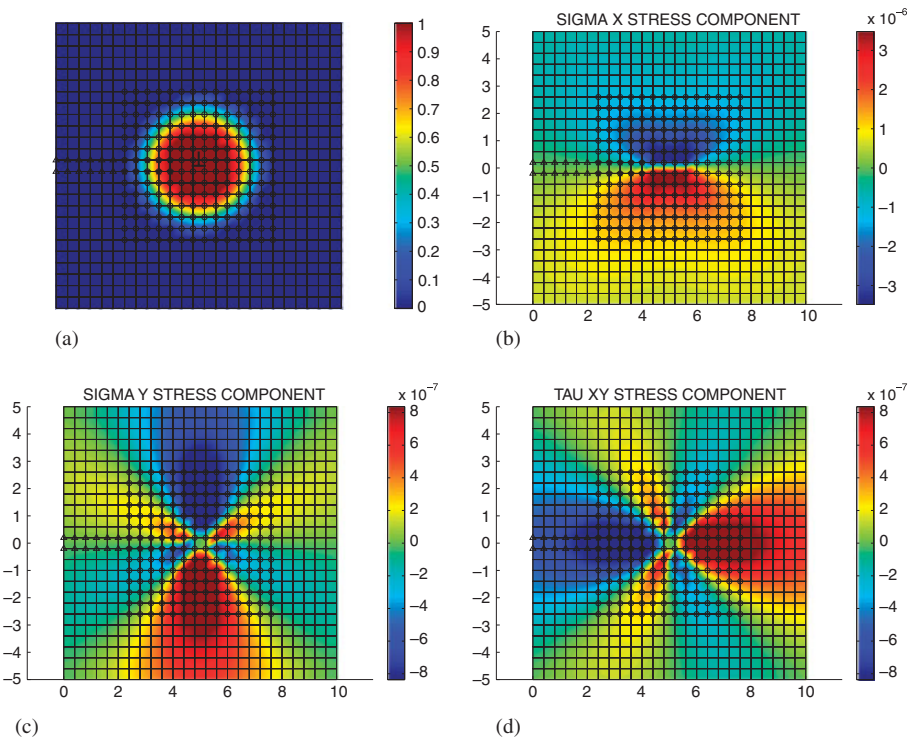

Figure 14. Results for the dislocation problem, enrichment type DOL+H: (a) weight function and (b–d) normal and tangential stress. The results are computed with ramp exponent $n=1$, a constant plateau of 3 layers of elements and a total of 6 enrichment layers.

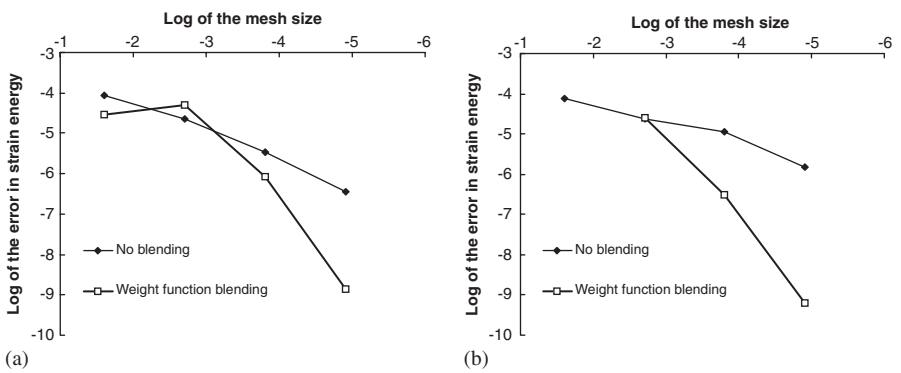

Figure 15. Convergence of the two considered enrichment methods: (a) DOL+H and (b) DOL.

ramp weight function with a constant plateau of one layer of elements around the tip were used, i.e. $d_e=2$ layers and $d_i=1$ layer. In Figure 16, hollow triangles denote Heaviside enriched nodes, while hollow circles represent nodes enriched with the analytic asymptotic solution (30). Note that

DOI: 10.1002/nme

Table I. Convergence rates for the dislocation problem with and without weight function blending and the three examined enrichment schemes.

Enrichment scheme	EEL	DOL	DOL+H
No blending	0.67	0.50	0.73
Weight function blending	2.18	2.09	2.08

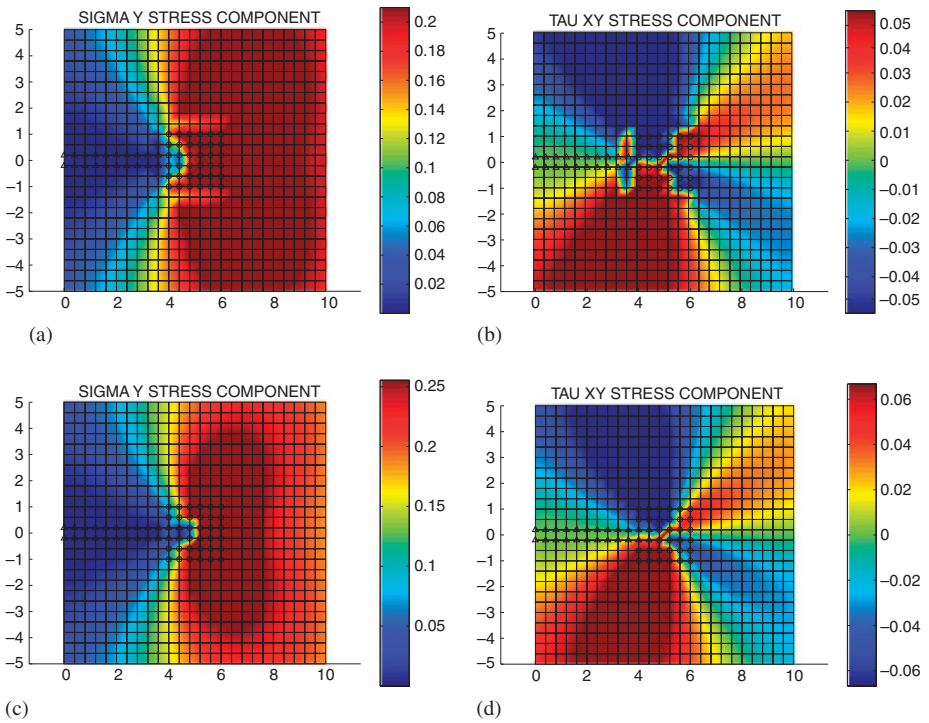

Figure 16. Results for the crack problem. Hollow triangles represent Heaviside step function enrichment, while hollow circles are nodes with the asymptotic solution enrichment. The left column is the vertical (σ_y) stress and on the right the shear stress τ_{xy}. On the top row no blending weight function was used. On the bottom row a linear ramp weight function with a constant plateau of one layer of elements around the crack tip was considered. The crack tip is at the center and the crack line extends horizontally on the left.

all nodes enriched with the asymptotic solution share the same enrichment degree of freedom K_I. No weight function derivatives have been considered in the computation of the stiffness matrix because, as will be shown, they can adversely affect the results.

In Figure 16, the top row illustrates the results of a standard XFEM implementation of crack analysis: some nodes around the crack tip are enriched with the asymptotic solution and the Heaviside step function is used for the remaining part of the crack (horizontal, toward left).

DOI: 10.1002/nme

Oscillations in the stress contours due to blending are clearly evident between unenriched elements and elements enriched by the asymptotic solution. In the bottom row of Figure 16, the proposed blending technique is employed; the reported contours are almost indistinguishable from the analytic solution.

A study of the weighted XFEM has been carried out by considering the following combination parameters in a mesh of 25×25 elements:

- 2 and 6 enrichment layers, to demonstrate the effectiveness of the method with few enrichment layers;
- weight function exponents $n = 1, 2, 4$, to confirm the lowest exponent gives superior results;
- the constant plateau distance d_i has been defined to contain $n_l/2$ layers of elements, where n_l is the number of enrichment layers;
- with and without the weight function derivatives in the evaluation of the strain.

The relative error in energy, compared with the analytic solution [40], is reported in Figure 17(a) and (b). The error in the stress intensity factor K_I has been reported in Figure 17(c) and (d).

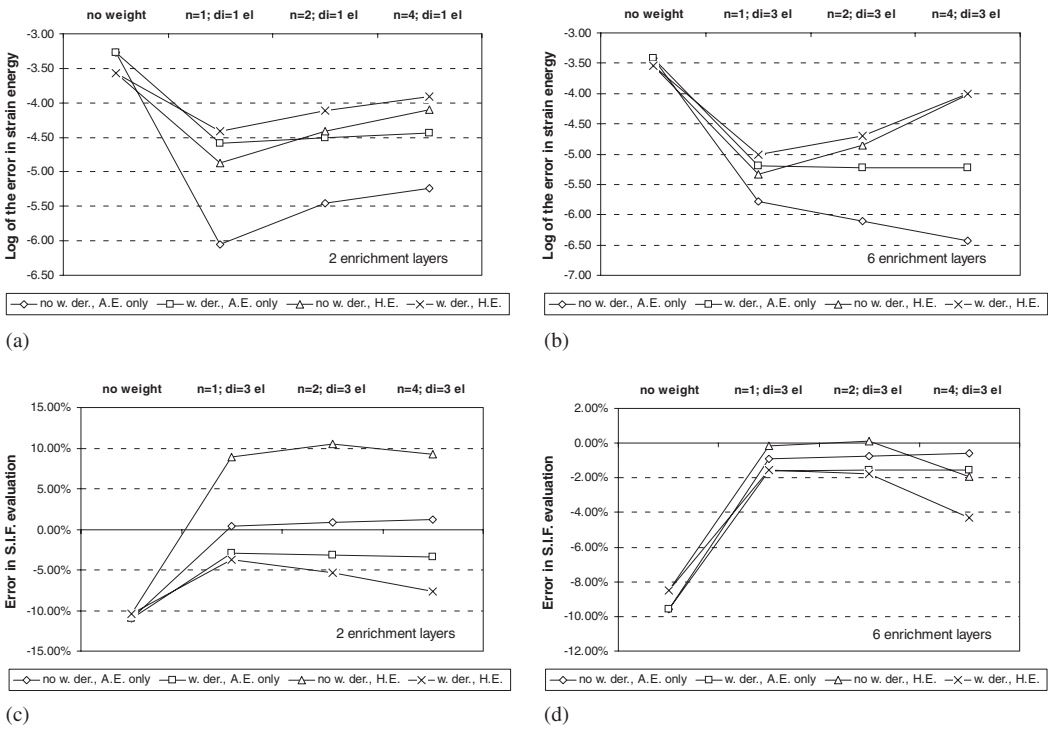

Figure 17. Relative error in energy (top row) and error in stress intensity factor (bottom row) for various ramp exponents. On the left 2 enrichment layers and on the right 6 enrichment layers. The graphs refer to the cases of analytic enrichment (A.E.) or analytic and Heaviside enrichment (H.E.), with and without considering weight function derivatives. The blending by weight function always significantly improves the result.

DOI: 10.1002/nme

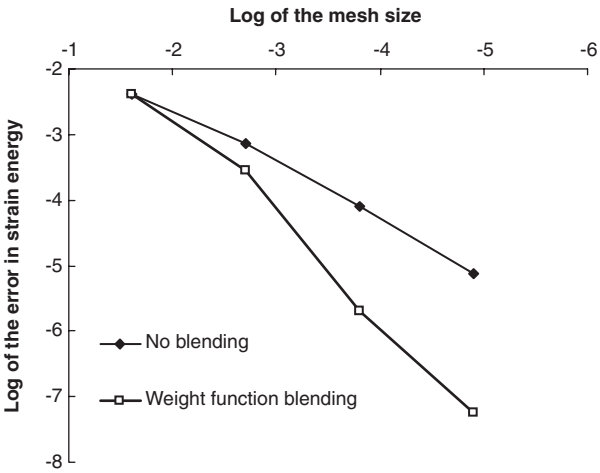

Figure 18. Convergence for the crack problem.

From the results in Figure 17, it can be seen that in all cases, the weighted XFEM is more accurate than the standard XFEM. More specifically, it is can be observed that

- the weight function exponent n does not play a significant role, so that a good choice is the linear ramp $n=1$;
- considering the weight function derivatives in the evaluation of strains usually worsens the results;
- the weighted XFEM does not require a large number of enrichment layers to perform very well (compare left and right columns of Figure 17).

Finally, a convergence analysis has been performed for the DOL+H enrichment scheme. Meshes from 5×5 to 135×135 elements with a constant enrichment subdomain have been considered (Figure 18). Again, a very significant improvement with the proposed weight function blending procedure is apparent. Considering the mean slopes of the three rightmost points of Figure 18, the convergence rate doubles, as the slope changes from 0.84 (no blending) to 1.68 (weight function blending).

9. CONCLUSIONS

We have presented a new method for the efficient numerical integration of the discrete equations of XFEM when the enrichment functions are self-equilibrating, i.e. when the enriched part of the displacement approximation satisfies equilibrium. The method is based on the transformation of the domain integrals of the discrete equations into boundary integrals. We have considered the more general case where the enrichment approximation is shifted to simplify the application of essential boundary conditions. The method is particularly effective when the enrichment function is singular or is not a polynomial, since standard Gauss quadrature is inefficient for such functions. The boundary integral method is compared with the sub-cell and nearly polar integrations methods for the case of the singular edge dislocation enrichment. It is shown that the boundary integration

DOI: 10.1002/nme

method requires only 32 quadrature points to obtain accurate solutions, while the nearly polar integration method requires over 300 points to obtain results with comparable accuracy.

We have also addressed the issue of reducing errors due to the blending of enriched and unenriched subdomains in XFEM. This work was motivated by our previous studies of dislocations [16, 41], where all the enriched degrees of freedom are equal. We have therefore focused our discussions in this paper to enrichments of this type. Our strategy involves premultiplying the enrichment function by a weight function with compact support as in the work of Fries [35]. The basic idea of this weighted XFEM is that the contribution of the enrichment to the solution of the problem is smoothly decreased, without introducing discontinuities or additional quadrature requirements. Therefore, in the vicinity of the feature being enriched, the weight function has a value of unity; away from the feature, it is smoothly decreased to zero by a C^0 polynomial. We have considered an unshifted approximation and two shifted approximations (type 1 and type 2 shifting).

When the weight function is chosen as a sum of a subset of the nodal shape functions (18), as proposed in [35] and when all the enriched degrees of freedom are constrained to be equal, the weighted approach degenerates to the standard XFEM. The degenerate case can be avoided by applying the weight function to a shifted enrichment function (what we have term type 2 shifting).

Numerical studies of dislocation and crack problems show that the weighted XFEM improves the accuracy of the XFEM. In addition, it converges optimally, even when the standard XFEM does not. This suggests that the parasitic terms in the approximation space of the blending elements have been removed. Our studies suggest that the optimal form of the weight function is a linear function, as used in [35], when the linear weight function is combined with a type 2 shifted approximation. Our studies also suggest that a better or almost equivalent quality approximation is obtained by *not considering* the weight function derivatives in the evaluation of the strains. In either case, the weighted XFEM always improves the solution.

Finally, both the proposed boundary integration method and the weighted XFEM approximation are easily implemented into existing XFEM codes and hence should be attractive options for improving both the efficiency and the accuracy of the method.

ACKNOWLEDGEMENTS

The support of the Office of Naval Research under Grant N00014-06-1-0505 and the Natural Sciences and Engineering Research Council of Canada under a Canada Graduate Scholarship is gratefully acknowledged.

REFERENCES

1. Belytschko T, Black T. Elastic crack growth in finite elements with minimal remeshing. *International Journal for Numerical Methods in Engineering* 1999; **45**:601–620.
2. Moës N, Dolbow J, Belytschko T. A finite element method for crack growth without remeshing. *International Journal for Numerical Methods in Engineering* 1999; **46**:131–150.
3. Strouboulis T, Babuška I, Copps T. The design and analysis of the generalized finite element method. *Computer Methods in Applied Mechanics and Engineering* 2000; **181**:43–69.
4. Duarte C, Babuška I, Oden J. Generalized finite element method for three-dimensional structural mechanics problems. *Computers and Structures* 2000; **77**:219–232.
5. Sukumar N, Chopp D, Moës N, Belytschko T. Modeling holes and inclusions by level sets in the extended finite element method. *Computer Methods in Applied Mechanics and Engineering* 2001; **90**:6183–6200.
6. Sukumar N, Moës N, Moran B, Belytschko T. Extended finite element method for three-dimensional crack modeling. *International Journal for Numerical Methods in Engineering* 2000; **48**:1549–1570.

DOI: 10.1002/nme

7. Gravouil A, Moës N, Belytschko T. Non-planar 3D crack growth by the extended finite element and level sets. Part II: level set update. *International Journal for Numerical Methods in Engineering* 2002; **53**:2569–2586.
8. Ventura G, Budyn E, Belytschko T. Vector level sets for description of propagating cracks in finite elements. *International Journal for Numerical Methods in Engineering* 2003; **58**:1571–1592.
9. Ventura G, Xu J, Belytschko T. A vector level set method and new discontinuity approximations for crack growth by EFG. *International Journal for Numerical Methods in Engineering* 2002; **54**:923–944.
10. Stolarska M, Chopp D, Moës N, Belytschko T. Modelling crack growth by level sets in the extended finite element method. *International Journal for Numerical Methods in Engineering* 2001; **51**:943–960.
11. Belytschko T, Moës N, Usui S, Parimi C. Arbitrary discontinuities in finite elements. *International Journal for Numerical Methods in Engineering* 2001; **50**:993–1013.
12. Chessa J, Smolinski P, Belytschko T. The extended finite element method for solidification problems. *International Journal for Numerical Methods in Engineering* 2002; **53**:1957–1977.
13. Asadpoure A, Mohammadi S. Developing new enrichment functions for crack simulation in orthotropic media by the extended finite element method. *International Journal for Numerical Methods in Engineering* 2007; **69**:2150–2172.
14. Areias P, Belytschko T. Two-scale shear band evolution by local partition of unity. *International Journal for Numerical Methods in Engineering* 2006; **66**:878–910.
15. Prabel B, Combescure A, Gravouil A, Marie S. Level set X-FEM non-matching meshes: application to dynamic crack propagation in elastic–plastic media. *International Journal for Numerical Methods in Engineering* 2007; **69**:1553–1569.
16. Ventura G, Moran B, Belytschko T. Dislocations by partition of unity. *International Journal for Numerical Methods in Engineering* 2005; **62**:1463–1487.
17. Gracie R, Ventura G, Belytschko T. A new fast finite element method for dislocations based on interior discontinuities. *International Journal for Numerical Methods in Engineering* 2007; **69**:423–441.
18. Bordas S, Nguyen P, Dunant C, Guidoum A, Nguyen-Dang H. An extended finite element library. *International Journal for Numerical Methods in Engineering* 2007; **71**:703–732.
19. Duflot M. A study of the representation of cracks with level sets. *International Journal for Numerical Methods in Engineering* 2007; **70**:1261–1302.
20. Belytschko T, Fish J, Engelmann BE. A finite element with embedded localization zones. *Computer Methods in Applied Mechanics and Engineering* 1988; **70**:59–89.
21. Fish J. The s-version of the finite element method. *Computers and Structures* 1992; **43**:539–547.
22. Fish J, Nath A. Adaptive and hierarchical modeling of fatigue crack propagation. *International Journal for Numerical Methods in Engineering* 1993; **36**:2825–2836.
23. Belytschko T, Fish J, Bayliss A. The spectral overlay on the finite element solutions with high gradients. *Computer Methods in Applied Mechanics and Engineering* 1990; **81**:71–89.
24. Melenk J, Babuska I. The partition of unity finite element method: basic theory and applications. *Computer Methods in Applied Mechanics and Engineering* 1996; **39**:289–314.
25. Lee S-H, Song J-H, Yoon Y-C, Zi G, Belytschko T. Combined extended and superimposed finite element method for cracks. *International Journal for Numerical Methods in Engineering* 2004; **59**:1119–1136.
26. Fish J, Yuan Z. Multiscale enrichment based on partition of unity. *International Journal for Numerical Methods in Engineering* 2005; **62**:1341–1359.
27. Fan R, Fish J. The rs-method for material failure simulations. *International Journal for Numerical Methods in Engineering* 2008; **73**:1607–1623.
28. Chessa J, Wang H, Belytschko T. On the construction of blending elements for local partition of unity enriched finite elements. *International Journal for Numerical Methods in Engineering* 2003; **57**:1015–1038.
29. Stazi F, Budyn E, Chessa J, Belytschko T. An extended finite element method with higher-order elements for curved cracks. *Computational Mechanics* 2003; **31**:38–48.
30. Legay A, Wang H, Belytschko T. Strong and weak arbitrary discontinuities in spectral finite elements. *International Journal for Numerical Methods in Engineering* 2005; **64**:991–1008.
31. Gracie R, Wang H, Belytschko T. Blending in the extended finite element method by discontinuous Galerkin and assumed strain methods. *International Journal for Numerical Methods in Engineering* 2007; DOI: 10.1002/nme.2217.
32. Tarancòn JE, Vercher A, Giner E, Fuenmayor FJ. Enhanced blending elements for XFEM applied to linear elastic fracture mechanics. *International Journal for Numerical Methods in Engineering* 2008; DOI: 10.1002/nme.2402.
33. Fries T, Belytschko T. The intrinsic XFEM: a method for arbitrary discontinuities without additional unknowns. *International Journal for Numerical Methods in Engineering* 2006; **68**:1358–1385.

34. Farhat C, Harari I, Franca LP. The discontinuous enrichment method. *Computer Methods in Applied Mechanics and Engineering* 2001; **190**:6455–6479.
35. Fries T. A corrected XFEM approximation without problems in blending elements. *International Journal for Numerical Methods in Engineering* 2007; DOI: 10.1002/nme.2259.
36. Laborde P, Pommier J, Renard Y, Salaun M. High-order extended finite element method for cracked domains. *International Journal for Numerical Methods in Engineering* 2005; **64**:354–381.
37. Gifford LN, Hilton PD. Stress intensity factors by enriched finite elements. *Engineering Fracture Mechanics* 1978; **10**:485–496.
38. Béchet E, Minnebo H, Moës N, Burgardt B. Improved implementation and robustness study of the X-FEM for stress analysis around cracks. *International Journal for Numerical Methods in Engineering* 2005; **64**:1033–1056.
39. Ventura G. On the elimination of quadrature subcells for discontinuous functions in the extended finite-element method. *International Journal for Numerical Methods in Engineering* 2006; **66**:761–795.
40. Liu X, Xiao Q, Karihaloo B. XFEM for direct evaluation of mixed mode SIFs in homogeneous and bi-materials. *International Journal for Numerical Methods in Engineering* 2004; **59**:1103–1118.
41. Gracie R, Oswald J, Belytschko T. On a new extended finite element method for dislocations: core enrichment and nonlinear formulation. *Journal of the Mechanics and Physics of Solids* 2008; **56**:200–214.
42. Hirth J, Lothe J. *Theory of Dislocations* (2nd edn). Wiley: New York, 1982.